

Design of an ecosystem to foster systemic eco-innovation. Systemic design for autopoietic local economies

Original

Design of an ecosystem to foster systemic eco-innovation. Systemic design for autopoietic local economies / Battistoni, C.; Barbero, S.. - In: FORMAKADEMISK. - ISSN 1890-9515. - ELETTRONICO. - 13:2, art.4(2020), pp. 1-23. [10.7577/formakademisk.3408]

Availability:

This version is available at: 11583/2765212 since: 2022-01-29T18:27:23Z

Publisher:

OsloMet - Oslo Metropolitan University

Published

DOI:10.7577/formakademisk.3408

Terms of use:

This article is made available under terms and conditions as specified in the corresponding bibliographic description in the repository

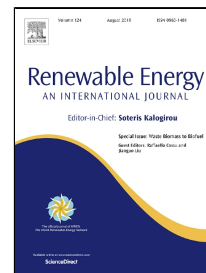
Publisher copyright

(Article begins on next page)

Accepted Manuscript

Catalytic Stability of a Ni-Catalyst Towards Biogas Reforming in the Presence of Deactivating Trace Compounds

Davide Papurello, Vitaliano Chiodo, Susanna Maisano, Andrea Lanzini, Massimo Santarelli



PII: S0960-1481(18)30525-1
DOI: 10.1016/j.renene.2018.05.006
Reference: RENE 10058
To appear in: *Renewable Energy*
Received Date: 23 June 2017
Revised Date: 27 March 2018
Accepted Date: 02 May 2018

Please cite this article as: Davide Papurello, Vitaliano Chiodo, Susanna Maisano, Andrea Lanzini, Massimo Santarelli, Catalytic Stability of a Ni-Catalyst Towards Biogas Reforming in the Presence of Deactivating Trace Compounds, *Renewable Energy* (2018), doi: 10.1016/j.renene.2018.05.006

This is a PDF file of an unedited manuscript that has been accepted for publication. As a service to our customers we are providing this early version of the manuscript. The manuscript will undergo copyediting, typesetting, and review of the resulting proof before it is published in its final form. Please note that during the production process errors may be discovered which could affect the content, and all legal disclaimers that apply to the journal pertain.

Catalytic stability of a Ni-catalyst towards biogas reforming in the presence of deactivating trace compounds

Davide Papurello^{b*}, Vitaliano Chiodo^a, Susanna Maisano^a, Andrea Lanzini^b, Massimo Santarelli^b

^a *Institute CNR-ITAE “Nicola Giordano”, Via S. Lucia sopra Contesse, 5 – 98126, Messina, Italy*

^b *Department of Energy, Politecnico di Torino, Corso Duca degli Abruzzi 24, 10129, Torino – Italy*

*Corresponding author. Tel.: +393402351692. Email address: davide.papurello@polito.it

Abstract

Trace compounds contained in the produced biogas range from tens to thousands of ppm(v) and the gas cleaning is crucial, as much as it is important the investigation of the trace compounds impact on the reforming section and on the SOFC performance. The catalytic stability of a Ni-catalyst towards biogas reforming in the presence of three types of deactivating compounds (sulfur, siloxanes and aromatic compounds) was investigated. When the biogas is composed of a methane to carbon dioxide ratio >1 under the tested operating conditions, the Ni catalyst stability is achieved. A Ni/Al₂O₃ catalyst appears suitable for the steam reforming of biogas including contaminants, under the operative conditions adopted. On the contrary, the effect of a biogas stream with composition CH₄/CO₂=50/50 vol. % is much more harmful under steam reforming conditions both in terms of activity and stability. This result was due to CO₂-promoted Boudouard reaction that leads to extensive carbon formation on the catalyst surface. Under this condition, sulfur and D5 compounds in the biogas have a significant impact on the longevity of the Ni catalyst. Hence, carbon formation rate is affected by the degree of catalyst poisoning due to adsorption and/or deposition of other species on catalytic sites.

Keywords:

Catalytic stability, biogas, trace compounds, SOFC, Direct internal reforming

Nomenclature:

ASR, Area Specific Resistance;

CEM, Controlled Evaporator Mixer;

DIR, Direct Internal Reforming;

EIS, Electrochemical Impedance Spectroscopy;

FID, chromatography-Flame Ionization Detector;

FU, Fuel Utilization;

- 32 GC, Gas Chromatography;
- 33 GHSV, Gas Hourly Space Velocity;
- 34 LSCF, Lanthanum Strontium Cobalt Ferrite;
- 35 OFMSW, Organic Fraction Municipal Solid Waste;
- 36 ppb(v), parts per billion by volume;
- 37 ppm(v), parts per million by volume;
- 38 SEM, Scanning Electron Microscope;
- 39 SOFC, Solid Oxide Fuel Cell;
- 40 TAR, dark brown or black viscous liquid of hydrocarbons
- 41 TCD, gas chromatography-Thermal Conductivity Detector;
- 42 TEM, Transmission Electron Microscope;
- 43 TPB, Three Phase Boundary;
- 44 WWTP, Waste Water Treatment plant;
- 45 YSZ, Ytria-Stabilized Zirconia.

46

47

48

49

50

51

52

53

54

55

56

57

58 *1. Introduction*

59 Biogas coming from the anaerobic digestion of organic waste covers a crucial role regarding landfilling
60 and pollutant reduction, matter recovery and energy production. Putrescible waste can derive from the
61 domestic urban organic waste, agricultural waste, manure and sludge collected in wastewater treatment
62 plants. Biogas consists of CH₄ (45-70 vol. %), CO₂ (30-50 vol. %), N₂ (<5 vol. %), O₂ (0-3 vol. %) and a
63 wide variety of trace compounds. The type and quantity of trace compounds depend on waste treated [1–4].
64 In fact, trace compounds found in landfill biogas and from digestion of organic wastes are completely
65 different [1,5]. Landfill gas quality is widely varying depending on the degradation status of the landfilled
66 material as well as moisture and temperature conditions, all of which may vary considerably in different parts
67 of the landfill body [5]. The higher amount of aromatic compounds found in landfill biogas compared to
68 sewage or farm biogases is often associated with older waste even though elevated levels of aromatic
69 compounds have also been measured in urban waste disposal bins [6–8]. The main trace compound
70 contained in a biogas from the anaerobic digestion of organic wastes – both from WWTPs or municipal
71 organic waste – is hydrogen sulfide (H₂S) [1,5,9]. The H₂S concentration can range from 10 to thousands of
72 ppm(v), and it is a function of the organic waste, digester temperature and pre-treatments process adopted to
73 improve the methane yield [1,10]. Some pre-treatments can be adopted during the biogas production to
74 reduce the sulfur content in the biogas, such as processes with metal oxides. Other processes are
75 implemented outside the digester, mainly processes that adopt the physical adsorption solution to abate trace
76 concentration [3,8,11–17]. Among energy generators, SOFCs are silent systems, with low emissions and
77 high electrical and thermal efficiency. These systems can produce energy in a distributed way and they can
78 be adopted in the next future to reduce the energy dependency from fossil fuels with high efficiency
79 [8,18,19]. The cleaning process of biogas results to be mandatory in order to reduce the trace contaminants to
80 achieve SOFC requirements [3,12,13,15,19–21]. A SOFC co-generator fed by biogas needs a reforming
81 process to produce a more suitable gas mixture rich in hydrogen and carbon monoxide content,
82 electrochemically suitable for the SOFC [22,23].

83 Biogas can be converted to synthesis gas either by dry reforming or by a combination of dry and steam
84 reforming using appropriate catalysts [24–27]. Since the CH₄ to CO₂ (molar) ratio in biogas is about 1.5, dry
85 reforming alone can lead to significant carbon deposition within the reactor [24,28,29]. Therefore, it is
86 desirable to mix biogas with steam for reforming and generally, the H₂O to CH₄ ratio (S/C) is maintained at 2
87 to avoid any coke formation [30,23,22]. Besides carbon deposition issues, the presence of impurities has a
88 tremendous effect on the performance of the catalyst. Among these, the most studied contaminant for
89 catalytic steam reforming is sulfur, in the form of H₂S, which leads to an almost total deactivation of the
90 catalyst [31–33]. Catalyst poisoning occurs due to the strong adsorption of sulfur or other impurities on
91 active sites, promoting by poisoning-metal electron affinity; this consequently, blocks or alters the
92 adsorptivity of the other species [34,35]. Overall, the saturation coverage of sulfur and other species (silicon
93 compounds) depends on the operating temperature, metal loading, and the partial pressure of reacting gasses.

94 Catalysts with lower metal loading lose activity at a faster rate compared to catalysts with higher metal
95 loading [36,37].

96 Moreover, the presence of higher molecular weight hydrocarbons (C_nH_m such as ethane, propane, etc.)
97 and aromatic compounds (benzene, toluene, etc.) can significantly affect the formation of carbon species and
98 thus the effectiveness of the catalyst [38,39]. The formation of carbon on the catalyst under steam reforming
99 conditions may take place mostly through cracking of hydrocarbons and aromatic compounds as well as the
100 Boudouard reaction. In this way, researchers [40,41] determined the coking tendency for steam reforming of
101 methane in the presence of C2 and C3 hydrocarbons over a Ni catalyst, and an increasing of coking with
102 carbon number was noted especially in the presence of olefin species. D'Angeli et al. [42] have also shown
103 that coke formation increases with the molecular weight of the feed and that the deactivation rates during
104 steam-reforming of ethane and propane over Ni/MgO were higher compared to methane.

105 Although poisoning of Ni in the presence of H_2S or hydrocarbons is well known, combined effects of
106 H_2S with other contaminants – which are the typical case of biogas – are lacking in the literature. Hence, the
107 main objectives of our research are:

- 108 i) to investigate the catalytic stability of a Ni-catalyst towards biogas reforming in the presence of
109 three types of deactivating compounds (H_2S , higher hydrocarbons, and siloxane compounds)
110 either alone or combined;
- 111 ii) to analyze the catalytic performances when different biogas compositions are used;
- 112 iii) to evaluate reforming options to increase catalyst lifetime and/or reduce the reformer operating
113 temperature;
- 114 iv) to find the best performance regarding carbon deposition and voltage stability in an SOFC single
115 cell fed with a mixture that simulates the direct internal reforming of biogas;
- 116 v) to investigate the SOFC performance fed by biogas with different trace compounds, starting
117 from sulfur compounds (H_2S) to continue with the addition of siloxanes (D4) and aromatic
118 compounds (C_7H_8).

119 The novelty of the paper, from the catalytic point of view, can be identified mainly on two aspects. The
120 first aspect is related to the combined effect of biogas contaminants on Ni catalytic stability; while the
121 second one is the performance evaluation of biogas contaminants depending on biogas stream composition in
122 terms of CH_4/CO_2 inlet ratio.

123

124 2. Experimental

125 2.1. Catalytic experiments on the reformer Ni catalyst

126 Catalytic experiments were carried out in a quartz fixed-bed reactor (i.d. = 4 mm; $h_{\text{bed}} = 2.0\text{--}4.0$ cm) at
 127 1073 K and atmospheric pressure. 0.2 g of commercial Ni/Al₂O₃ reforming catalyst [28,22,43]. The
 128 operative temperature in the reactor was assured by three thermocouples located in different zones of the
 129 catalytic bed. Before each test run, catalysts were reduced in-situ at T=1073 K for 1.5 h under hydrogen flow
 130 (100 cc/min).

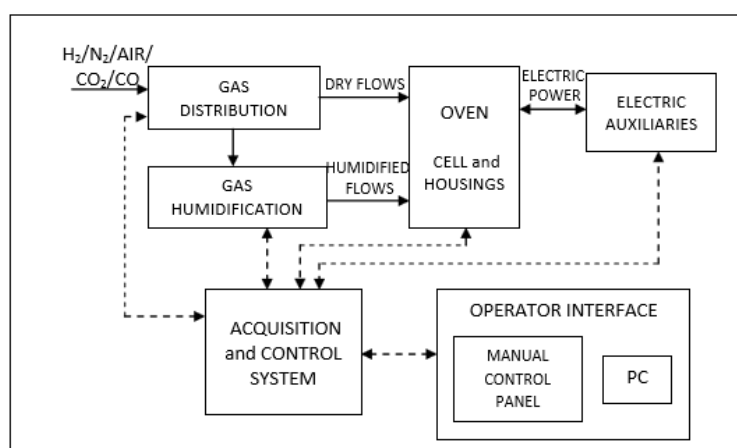
131 The flow rates of biogas (CH₄+CO₂) and poisoning species (H₂S, hydrocarbons, and siloxane) were
 132 controlled by Brooks Instruments mass flow meters. In particular, the following poisoning concentrations
 133 ranges were added in the reactant mixture: i) H₂S=0.4-1 ppm(v), ii) Decamethylcyclopentasiloxane (D5-
 134 siloxane, C₁₀H₃₀O₅Si₅=0.5-1 ppm(v) and iii) hydrocarbons mixture=200-800 ppm(v)

135 Carbon formation during experiments was estimated by using a CHSN-O Carlo Erba elementary
 136 analysis instrument, while A PHILIPS CM12 Transmission Electron Microscope (TEM) provided with a
 137 high-resolution camera was used to analyze the morphology of both fresh and spent Ni catalysts. A field
 138 emission Scanning Electron Microscope (SEM) equipped with EDAX microprobe (Philips XL30 S FEG)
 139 was used to carry out qualitative and quantitative analysis of solid compounds (i.e., SiO₂) on the powders of
 140 spent Ni catalysts.

141 2.2. Electrochemical characterization of SOFC single cells

142 Single SOFC cells were tested with simulated biogas to investigate the effects of direct internal
 143 reforming and fuel contamination on the electrochemical performance of the fuel cell.

144 The laboratory test station is designed to test the planar SOFCs. A schematic diagram of the test rig is
 145 provided in Figure 1. The test rig includes an oven, in which ceramic housings holding the planar cell are
 146 placed. Moreover includes a gas mixing and distribution system; a humidification system, in which water is
 147 added to dry gaseous streams; electric auxiliaries, which supply electricity to the oven and to the cell.
 148 Finally, a data acquisition and control system is used to control the system.



149

150 *Figure 1. Schematic diagram of the test-rig. Solid lines indicate mass and energy streams, while dashed lines*
 151 *indicate data exchange between the acquisition and control system and the other subsystems.*

152 Two sintered alumina circular housings (diameter 80 mm) are located inside the oven. During
 153 experiments, the tested cell is placed between the housings which provide gas distribution to both cell
 154 electrodes and connect the cell to an external electronic load. The SOFC adopted in the tests is a planar
 155 anode supported fuel cell. The cell is composed by a porous YSZ anode plus a support layer, a dense
 156 electrolyte and a porous cathode made with LSCF. The cell has a circular section with an active surface of 47
 157 cm^2 (it means a radius of about 3.86 cm) and the thicknesses of the different layers are reported in Table 1.
 158 More detail on the experimental set-up can be found elsewhere [20,32,33,44].

159 *Table 1. Geometrical and material characteristics of the SOFC.*

Layer	Material	Thickness
Anode (Support+ Active layers)	Ni/8YSZ	517 μm
Electrolyte	YSZ	5 μm
Cathode	LSCF	45 μm

160 The gas distribution system connects the test-rig to laboratory gas manifolds and ensures that dry gas
 161 streams with specified flow rates and compositions are sent to the humidification system or directly to the
 162 cell. This system is composed by pipes, valves (Swagelok), mass flow controllers (Bronkhorst) and a
 163 Controlled Evaporator Mixer (CEM).

164

165 3. Results

166 3.1. Boundary concentration of biogas poisoning on reformer section

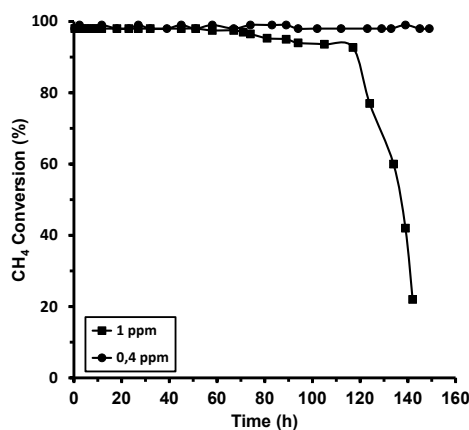
167 3.1.1. H_2S poisoning

168 Sulfur is known as harmful species for Ni based catalysts and it's hardly to inhibit the catalyst poisoning
 169 without specific experimental feedings [31,45]. Hence, the effect of H_2S poisoning on the Ni catalyst
 170 performance has been analyzed with respect to different concentrations (0.4 ppm(v) and 1 ppm(v)) in the
 171 inlet gas stream. Previously, a catalytic steam reforming test was performed with a "clean" biogas stream in
 172 order to verify the catalyst behavior in terms of carbon formation rate without poisoning.

173 Results in terms of methane conversion are shown for 0.4 and 1.0 ppm(v) of H_2S concentration in the
 174 fuel feed, respectively (Figure 2). The catalyst was stable for 150 hours of test with a GHSV of 15,000 h^{-1}
 175 when H_2S concentration was 0.4 ppm(v). In the experiment with 1 ppm(v) of H_2S , the Ni activity resulted in
 176 a fast deactivation after about 60 hours of stable operation. The CH_4 conversion dropped down rapidly from
 177 about 99% to 20%. This behavior would indicate that the breakthrough time is driven by sulfur concentration
 178 in the reactant gas mixture. Furthermore, analysis performed on "used" Ni catalysts through a CHNS
 179 analyzer, highlighted low rates of carbon formation ($\leq 0.1 \text{ mgC/g}_{\text{cat}}\cdot\text{h}$) as well as on Ni catalysts working with
 180 a clean biogas stream. This means that under the examined experimental conditions and 150 hours of time on

181 stream, the methane conversion rates are not affected by the poor carbon amounts deposited on catalyst
 182 surfaces.

183



184

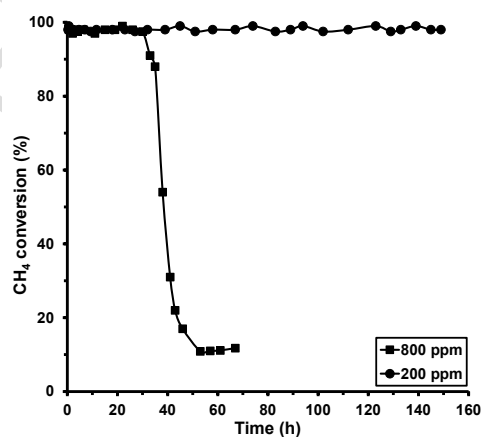
185 *Figure 2. Methane conversion vs time with H₂S poisoning: CH₄/CO₂=60/40 mol%; H₂O/CH₄= 2 mol/mol;*
 186 *GHSV=15,000 h⁻¹; T=1073 K; P=1 bar.*

187

3.1.2. Deactivation effects from heavier hydrocarbons

188 Generally, the reasons for deactivation of a Ni-based catalyst for the reforming of hydrocarbons are
 189 primarily due to carbon deposition promoted by unsaturated compounds (i.e. olefins, aromatics, etc.). Thus,
 190 effects of C₂ and C₃ species on Ni performances have been investigated through steam reforming
 191 experiments performed in presence of different hydrocarbons concentrations the biogas stream.

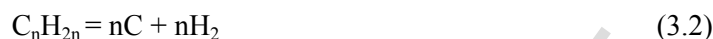
192 Results showed a dramatically reduction of the methane conversion rate from about 99% to about 10%
 193 after 50 h of time on stream in presence of an hydrocarbons concentration of 800 ppm(v) (calculated on
 194 biogas stream under dry condition) (see Figure3), while a total concentration of C₂ and C₃ compounds of 200
 195 ppm(v) would seem to have had no effect on the catalyst stability for 150 hours.



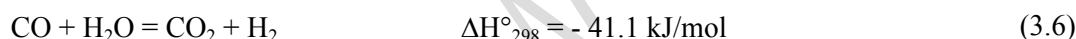
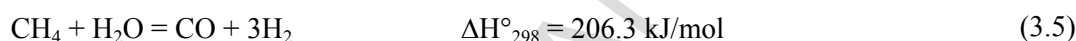
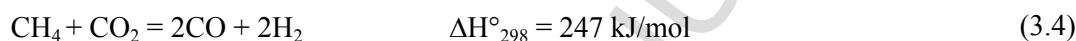
196

197 *Figure 3. Methane conversion vs time with higher hydrocarbons mixture addition: CH₄/CO₂=60/40 mol%;*
 198 *H₂O/CH₄= 2 mol/mol; GHSV=15,000 h⁻¹; T=1073 K; P=1 bar.*

199 The different Ni catalyst behaviors shown in Figure 3, could be mainly explainable by equilibrium
200 coking production (Eqs. 3.1,3.2 and 3.3).



201 In fact, the contribution of reaction 3.1, should increase with the increasing of heterogenous compounds
202 to avoid massive coke deposition promoted by pyrolysis of species with carbon number >1 (Eq. 3.2) [39].
203 Nevertheless, an excessive presence of harmful species (i.e. alkenes) could exert a substantial effect on coke
204 formation pathway [46]. In this context, it can be supposed that working with moderate poisoning
205 concentrations (≤ 200 ppm(v)) and under the conditions considered, an equilibrium among the main reactions
206 of the process has been achieved (Eqs. 3.4-3.6).



207 Data obtained by elementary analysis seem to confirm the above hypothesis; indeed a marked carbon
208 formation (about $0.39 \text{ mgC/g}_{\text{cat}}\cdot\text{h}$ after 70 hours of test) was detected on spent Ni sample working with 800
209 ppm(v) of hydrocarbons poisoning (Table 2), while a minor carbon deposition ($0.15 \text{ mgC/g}_{\text{cat}}\cdot\text{h}$) was
210 observed on Ni catalyst exposed to an hydrocarbons concentration of 200 ppm(v), as shown in Table 2.

211 *Table 2. Carbon and SiOx formation rates on spent Ni/Al₂O₃ catalysts: CH₄/CO₂=60/40 mol%; H₂O/CH₄= 2*
212 *mol/mol; GHSV=15,000 h⁻¹; T=1073 K; P=1 bar.*

	Hydrocarbons mixture*		D5 Siloxane	
Inlet gas concentration [ppm(v)]	800	200	1	0.5
Time on stream [h]	70	150	100	150
CH₄ conversion [mol%]	10	99	70	99
C formation rate [mgC/g_{cat}·h]	0.39	0.15	≤ 0.1	≤ 0.1
SiO₂ [wt%]	-	-	4.8	2.0

213 * Ethane, Ethylene, Acetylene, Propylene (200 ppm(v) for each)

214 3.1.3. Siloxanes poisoning

215 Experiments were performed adding to the inlet gas stream different concentrations of decamethyl-
216 cyclopenta-siloxane (D5) as the selected siloxane model compound. Results in terms of methane conversion

217 highlighted a decreasing of the Ni activity (from 99% to 70% after about 100 hours) when a concentration of
218 1 ppm(v) was added in the inlet gas stream. On the contrary, D5 concentration of 0.5 ppm(v) leaved
219 unchanged the methane conversion rate for 150 hours.

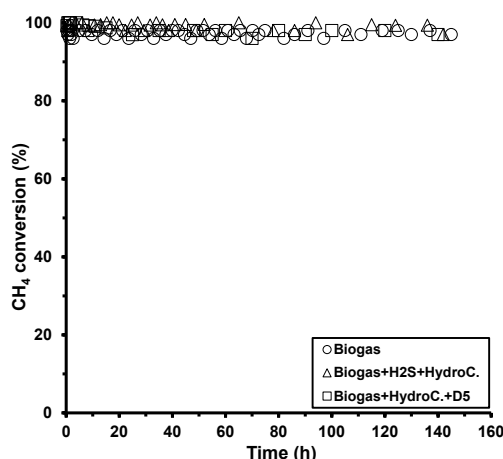
220 The Ni behavior can be attributed to its physical interaction with siloxanes compounds. In fact, D5
221 decomposes to SiO₂, which deposits on the catalyst surface compromising the catalytic activity (a similar
222 mechanism has been observed for the Ni-anode of the SOFC when exposed to D4 or D5 [47,48]). As
223 previously observed for spent Ni catalysts operated in presence of H₂S, the Ni samples exposed to different
224 D5 concentrations results minimally affected by carbon deposition (Table 2). While depositions of silicon
225 oxide were recorded on used Ni catalysts through SEM-EDAX analysis. As expected, the quantitative
226 analysis showed higher SiO₂(s) formation on Ni samples operated with 1 ppm(v) of D5 (SiO₂ = 4.8 wt. %)
227 than samples exposed to 0.5 ppm(v) of D5 (SiO₂ = 2.0 wt.%). These results are in according with recently
228 studies carried out by authors that detected remarkable micro-silica deposits (SiO₂) on Ni spent catalyst
229 exposed to D5 effect under biogas steam reforming reaction [42].

230 **3.1.4. Co-poisoning effect**

231 In order to investigate on possible synergic effects of co-feeding of harmful compounds on the Ni
232 catalyst stability versus time, two kinds of poisoning were added simultaneously in the inlet gas stream
233 ('H₂S+Hydrocarbons mix' and 'Hydrocarbons mix+D5', respectively). Hence, maximum boundary
234 concentrations of each contaminant (0.4 ppm(v), 200 ppm(v) and 0.5 ppm(v) for H₂S, hydrocarbons and D5,
235 respectively) were mixed with the biogas stream.

236 Results given in Figure 4 show that the performances of the Ni catalyst did not suffer deactivation under
237 the simultaneous presence of two different kinds of poisoning species, at the concentrations examined
238 (H₂S=0.4 ppm(v)+Hydrocarbons=200 ppm(v) and Hydrocarbons=200 ppm(v)+D5=0.5 ppm(v)), when the
239 molar ratio CH₄/CO₂=60%/40% was used. The catalytic stability was recorded for about 150 hours for each
240 test; a methane conversion rate of about 99% was detected both in the presence of 'H₂S+Hydrocarbons' and
241 'Hydrocarbons+D5' mixtures in the inlet gas stream.

242 Looking at the reformat gas compositions, the outlet molar fractions are very close to what is expected
243 from thermodynamic equilibrium, with an H₂/CO molar ratio about 2.3 mol/mol (see Table 3).



244

245 *Figure 4. Methane conversion vs time: $CH_4/CO_2=60/40$ mol%; $H_2O/CH_4=2$ mol/mol; $GHSV=15,000$ h^{-1} ;*
 246 *$T=1073$ K; $P=1$ bar.*

247 *Table 3. Outlet stream composition: $CH_4/CO_2=60/40$ mol%; $H_2O/CH_4=2$ mol/mol; $GHSV=15,000$ h^{-1} ;*
 248 *$T=1073$ K; $P=1$ bar.*

Outlet stream	Thermodynamic Equilibrium	Experimental
	[Vol. %]	
H ₂	49.8	48.3
CO	20.0	20.7
CO ₂	9.1	11.5
CH ₄	0.1	0.3
H ₂ O	21.0	19.2

249 **3.1.5. Impact of the inlet gas stream composition on biogas reforming**

250 **3.1.5.1. Effect of carbon dioxide concentration**

251 The influence of the CH_4/CO_2 ratio in the inlet gas stream on the Ni catalyst behavior was examined at
 252 1073 K, $H_2O/CH_4=2$ mol/mol; 15,000 h^{-1} of GHSV and atmospheric pressure. Experiments were repeated for
 253 50/50 mol% CH_4/CO_2 working both without and with the presence of poisoning in the biogas stream. Stable
 254 catalytic performance (about 140 hours) was observed when using clean biogas. In the presence of
 255 impurities, deactivation occurred. By adding the hydrocarbons mixture in the feed gas the methane
 256 conversion dropped from 98% to 86% after ~80 hours of operation with stable performance; the loss of
 257 catalytic activity vs. time was more evident when either H₂S or D5 were inserted in the inlet gas stream (CH_4
 258 conversion dropped from 98% to about 30% after 70 and 90 hours for H₂S and D5, respectively).

259 Finally, co-poisoning exposure under this 50/50 mol% CH_4/CO_2 mixture resulted in the worst condition
 260 in terms of catalyst stability with time. The two investigated combinations (H₂S+hydrocarbons and
 261 hydrocarbons+D5) resulted in a loss of Ni catalytic activity after only 20 hours of operation (see Figure 5).
 262 From the outlet stream composition, as reported in Table 4, an H₂/CO molar ratio close to 2.1 mol/mol was
 263 obtained during the stable operation phase (CH_4 conversion rate=98%).

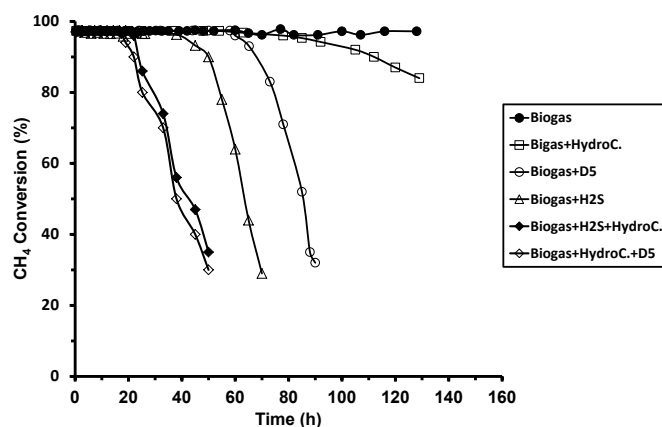


Figure 5. Methane conversion over time in the presence of different poisoning exposures: $CH_4/CO_2=50/50\text{mol}\%$; $H_2O/CH_4=2\text{ mol/mol}$; $GHSV=15,000\text{ h}^{-1}$; $T=1073\text{ K}$; $P=1\text{ bar}$.

Table 4. Outlet stream composition: $CH_4/CO_2=50/50\text{mol}\%$; $H_2O/CH_4=2\text{ mol/mol}$; $GHSV=15,000\text{ h}^{-1}$; $T=1073\text{ K}$; $P=1\text{ bar}$.

Outlet stream	Experimental [Vol. %]
H_2	45.1
CO	21.4
CO_2	12.8
CH_4	0.4
H_2O	20.3

The results from Figure 5, compared with the Ni catalyst performance reported in Figure 4, suggest that a decrease of the CH_4/CO_2 molar ratio in the biogas stream strongly induces negative effects on the Ni catalyst endurance. Moreover, the selectivity to H_2 production was reduced while the CO formation was favored. This behavior is probably due to the reverse WGS reaction ($CO_2+H_2=CO+H_2O$) promoted by carbon dioxide absorption on Ni catalyst active sites [43,44]. However, this means that coke formation by CO dissociation through the Boudouard reaction ($2CO=C+CO_2$) is favored, affecting in this way the catalyst endurance. In addition, the Ni catalyst efficiency in a 50/50 vol% CH_4/CO_2 stream, compared to a 60/40 mixture, was more vulnerable to the presence of contaminants. Especially, the co-feeding cases were now clearly more severe than the cases with only a single poison in the biogas stream.

3.1.6. Catalyst post-test characterization

3.1.6.1. Carbon formation rate

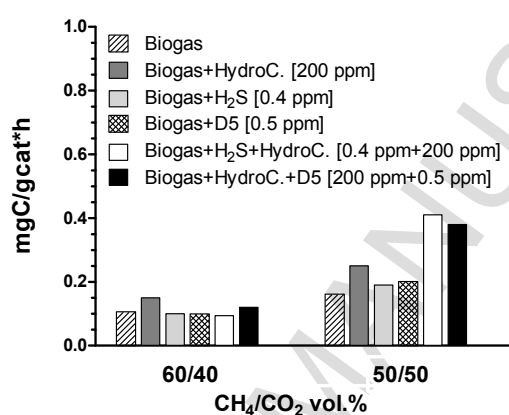
Different samples of spent catalysts were analyzed by CHSN elementary analysis to better understand the fundamental degradation mechanisms of catalytic steam reforming in the presence of impurities.

Results in Figure 6 show how the coke formation rate increased by increasing the carbon dioxide concentration in the biogas composition. A deposition rate of about $0.41\text{ mgC/g}_{\text{cat}}\cdot\text{h}$ was estimated for the mixture $CH_4/CO_2=50/50\text{ vol}\%$ (under co-poisoning conditions). This observation seems to confirm that the

286 earlier hypothesis of competitive adsorption of carbon dioxide and H₂O molecules on Ni active sites that
 287 leave to carbon formation probably promoted by CO dissociation through the Boudouard reaction
 288 (Eq.3.3). On the contrary, a biogas composition of CH₄/CO₂=60/40 vol% ensured stable catalyst performance
 289 for about 150 hours at a GHSV of 15,000 h⁻¹, also under co-poisoning conditions.

290 According to literature [45,46], these results allow some considerations on the effect of sulfur and D5 on
 291 carbon formation during the biogas steam reforming reaction. Indeed, experimental data indicate that the
 292 carbon deposition rate can be accelerated by the presence of contaminants in the biogas stream: the
 293 adsorption/precipitation of chemical poisoning species (e.g., sulfur and SiO₂) on the catalytic surface might
 294 inhibit the carbon regasification with steam that protects the metallic phase from coke deposition.

295
 296

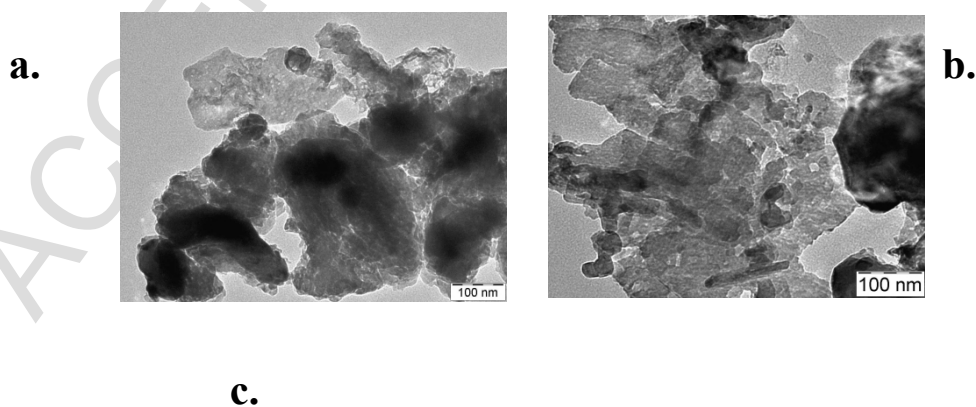


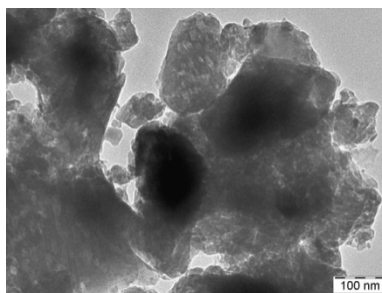
297
 298 *Figure 6. Coke formation rate on spent samples catalyst: GHSV=15,000 h⁻¹; 1073K.*

299 3.1.6.2. TEM and SEM microscopy evidences

300 To evaluate carbon deposits, TEM micrographs have been taken on spent catalyst samples. TEM images
 301 showed no evidence of large coke deposition when the feed gas was CH₄/CO₂=60/40 vol%. This result
 302 agrees with the catalytic data previously reported, which showed only modest coke formation rates.

303



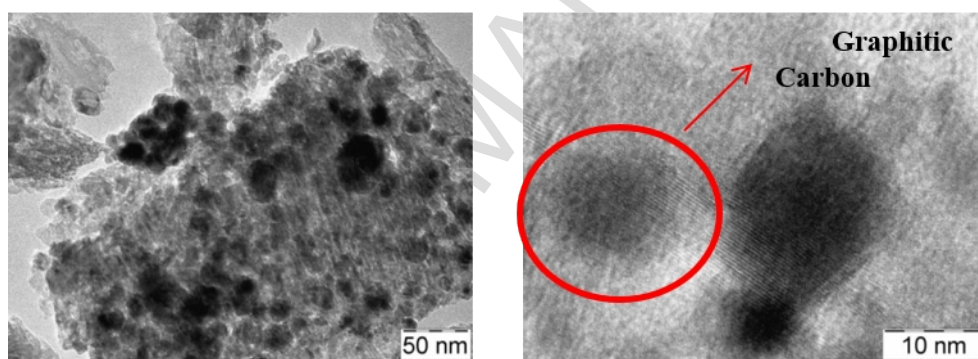


306
307
308
309
310

Figure 7. TEM images on fresh and spent catalysts: a) Ni catalyst “fresh”; b) Ni catalyst “used” $CH_4/CO_2=60/40$ mol%+ H_2S +HydroC.; $H_2O/CH_4=2$ mol/mol; $GHSV=15,000$ h^{-1} ; $T=1073$ K; $P=1$ bar; c) Ni catalyst “used” $CH_4/CO_2=60/40$ mol%+HydroC.+D5; $H_2O/CH_4=2$ mol/mol; $GHSV=15,000$ h^{-1} ; $T=1073$ K; $P=1$ bar.

311 On the contrary, agglomerates of carbon depositions were observed on spent Ni catalysts working under
312 a biogas flow of $CH_4/CO_2=50/50$ vol%. As highlighted by TEM images (see Figure 8), graphitic carbon
313 deposits are present on the Ni surface. we suspect that the catalytic deactivation trends recorded during tests
314 with poisoning might be due to deactivation/degradation effects other than only carbon deposition (e.g.,
315 deposition/adsorption of foreign chemical compounds or atoms). Further evidence of this is presented in
316 section 3.

317



318
319
320

Figure 8. TEM images on spent Ni catalyst at different magnifications: Ni catalyst “used” $CH_4/CO_2=50/50$ mol%+ H_2S +HydroC.; $H_2O/CH_4=2$ mol/mol; $GHSV=15,000$ h^{-1} ; $T=1073$ K; $P=1$ bar.

321 SEM investigations were carried out in order to determine silicon oxide deposits on spent Ni catalyst
322 samples after exposure to D5 siloxane as a contaminant. As reported in Table 5, comparable concentrations
323 of SiO_2 were detected on catalyst samples used to reform biogas containing D5 in the inlet stream; however,
324 the durations of the experiments were not identical. The condition with biogas of $CH_4/CO_2=50/50\%$ was
325 more prone to deposit silica when normalized for the experiment duration.

326

Table 5: SEM-EDAX analysis on spent Ni catalysts: $T=1073$ K, $GHSV=15,000$ h^{-1} .

SEM-EDAX		Operating Condition		
SiO_2 (wt. %)	CH_4/CO_2 (vol. %)	Hydrocarbon mix. (ppm(v))	D5 (ppm(v))	Time on stream (h)
2.4	60/40	200	0.5	150
2.5	50/50	200	0.5	50

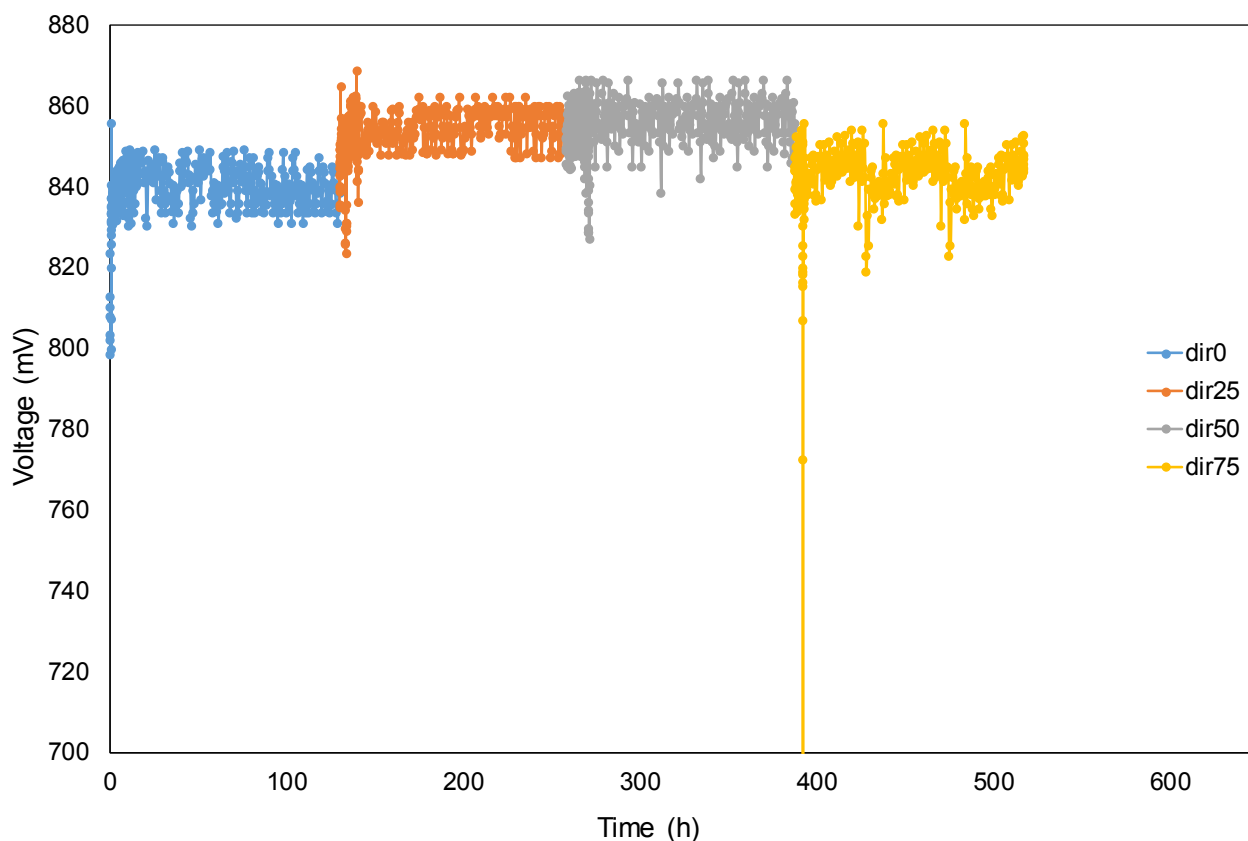
327 **3.2. SOFC single cell testing**328 **3.2.1. Direct internal reforming study**

329 The SOFC was fed by a gas mixture that simulates biogas fuel. The degree of direct internal reforming
 330 (DIR) of the biogas was varied from 0% (i.e., biogas is fully reformed externally before feeding the SOFC;
 331 in our experiments, we simulated directly the resulting reformat gas mixture) to 100% (in this case, the
 332 biogas is fully reformed inside the Ni-anode). Every experiment was carried out fixing the FU at 15% with a
 333 current density of 0.25 A/cm². The gas flow mixture of electrochemical fuel comes from the electrochemical
 334 hydrogen content, see the following table:

335 *Table 6. Biogas composition for different reforming degree.*

DIR (%)	H ₂ [mL/mi]	CH ₄ [mL/mi]	CO [mL/mi]	CO ₂ [mL/mi]	H ₂ O [mL/mi]	\dot{V}_{tot} [mL/mi]	T _{bubble} [°C]
0	346.2	6.6	184.8	40.9	58.7	637.1	49.6
25	220.3	54.9	117.6	59.8	88	540.6	64.2
50	127.5	90.5	68.1	73.75	109.6	469.5	75.3
75	56.4	117.8	30.1	84.85	126.2	414.9	87.4
100	0	139.4	0	92.9	139.4	371.7	93.5

336 In Figure 9, the voltage profile of the cell is given for the gas mixtures reported in Table 6. The cell voltage
 337 was quite stable during DIR 0, DIR 25 and DIR 50, while it oscillated at DIR 75. At DIR 100, technical
 338 limitations related to the maximum temperature achievable by the bubbler have reduced the voltage stability
 339 inducing the carbon deposition phenomena on the cell. At DIR 0%, an average voltage of 840 mV is
 340 attained, while at DIR 25 and at DIR 50, 850 mV and 860 mV are reached, respectively. The cell voltage
 341 increased up to DIR 50, which can be justified considering the calculated flows and the conditions that
 342 ideally should be present at the anode. Low H_2O/H_2 ratio allows to obtain a high-performance operation
 343 because reactants do not lower their partial pressure at the anode. At the same time a suitable H_2O/CH_4 ratio
 344 should be present because the reforming reactions take place.



345
346 *Figure 9. Voltage profile at different DIR condition.*

347 The best biogas condition to feed the cell in terms of stable performance is closer to DIR 50 condition with a
348 steam to methane and steam to hydrogen ratio comparable.

349 The Electrolyte Impedance Spectroscopy analyses are reported below. The cell monitoring has been
350 done at the beginning and at the end of the time intervals every 12 h.

351 The results of the EIS analysis are shown in Figure 10 providing a comparison of the Nyquist diagrams
352 obtained after 1 and 12 hours of operation in a given condition of DIR. The aim to reach in this phase is the
353 determination of the optimal external reforming able to find a compromise between the cell performance and
354 the economic impact.

355

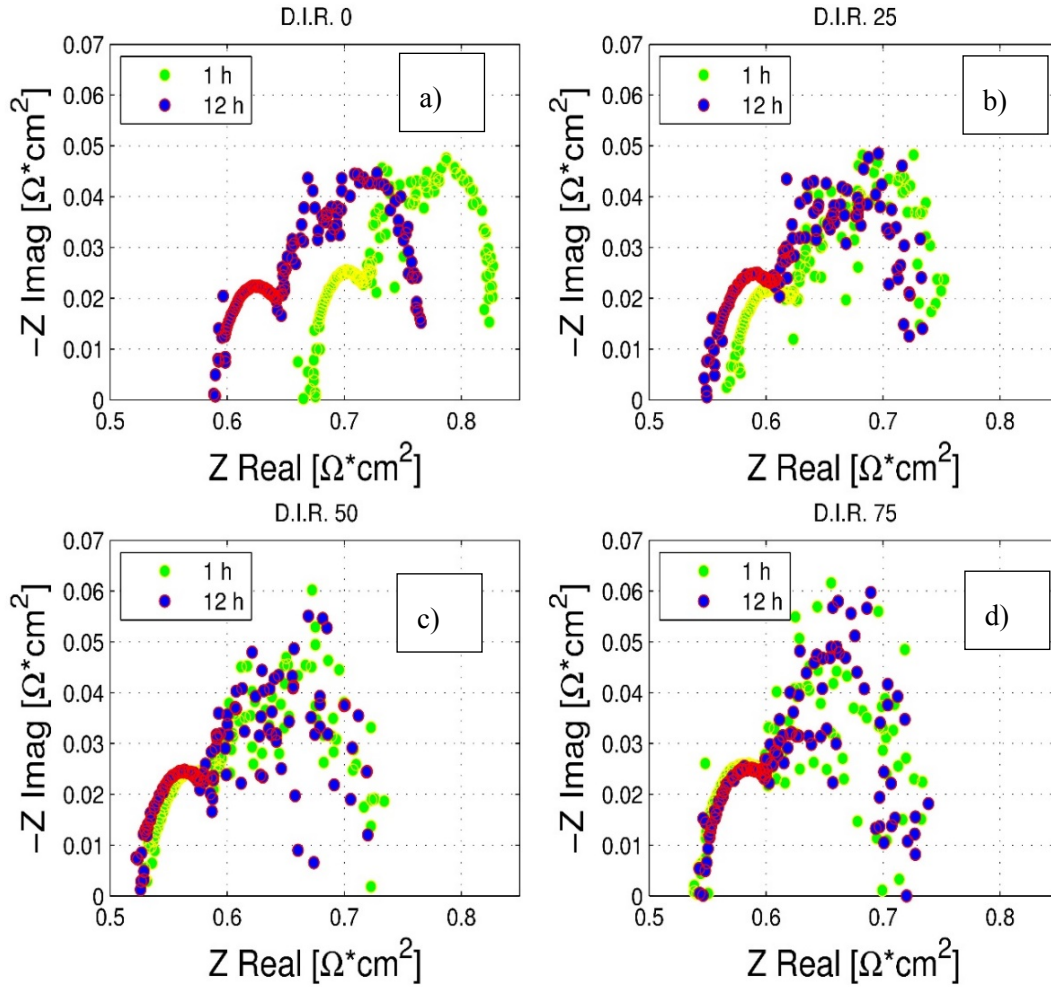


Figure 10. EIS results for different DIR.

Taking in consideration the electrochemical impedance spectroscopy analysis, the entity of the different losses can be extrapolated using the model reported elsewhere (see table 7) [20]:

Table 7. Cell losses during operation.

DIR	Time (h)	R_{ohm}	R_{el}	R_{transp}	R_p
		$[\Omega \cdot cm]$	$[\Omega \cdot cm]$	$[\Omega \cdot cm]$	$[\Omega \cdot cm]$
DIR0	1 h	0.67	0.07	0.11	0.83
DIR0	12 h	0.59	0.06	0.13	0.78
DIR 25	1 h	0.56	0.07	0.11	0.72
DIR 25	12 h	0.55	0.06	0.13	0.73
DIR 50	1 h	0.53	0.05	0.14	0.72
DIR 50	12 h	0.53	0.07	0.12	0.72

DIR 75	1 h	0.55	0.05	0.1	0.7
DIR 75	12 h	0.55	0.05	0.14	0.72

361 Observing the results reported above, the ohmic losses are not subjected to drastic variations in the 12 h
 362 of observation for almost all the DIR analyzed. The only exception is represented by the DIR 0. However,
 363 the main cause for the shift of the intersection with the real axis toward the left direction when the biogas
 364 exposure time increases is a temperature variation at which the cell has been undergone when the reformat
 365 biogas has been sent and this situation has increased the electrolyte conductivity.

366 The first arch of Nyquist plot, as previously discussed exemplifies the activation and the
 367 electrochemical losses, which are stable in DIR 50 and DIR 75, while in the other two analyzed
 368 configurations tend to decrease when the biogas's exposure time increases [15,47]. Finally, the low frequency
 369 arch of Nyquist plot has tendency to increase its extension towards higher DIR because, being this arch
 370 representative of the concentration losses, it has a higher impact where it is required to diffuse molecules
 371 with higher dimensions. This situation happens when the gas mixture is over powered in methane and carbon
 372 dioxide.

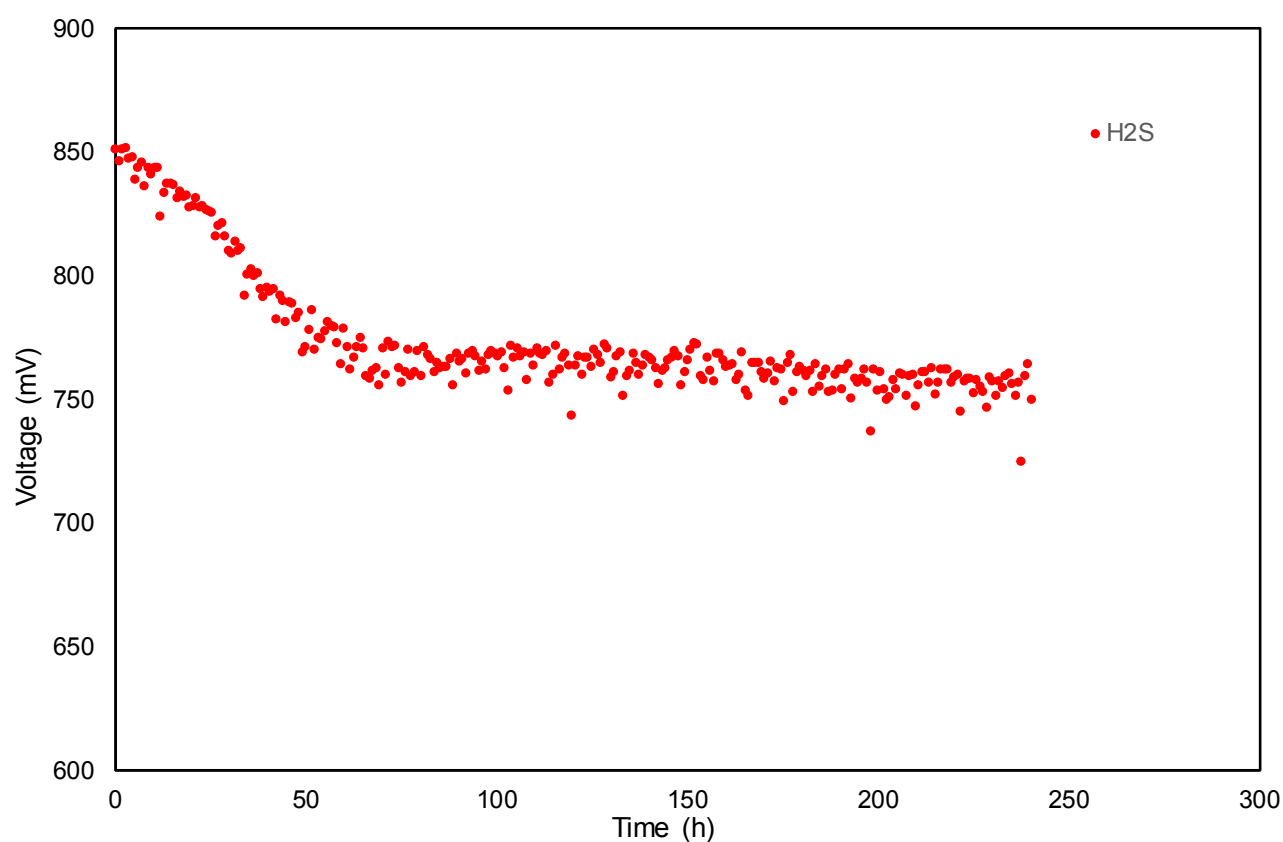
373 **3.2.2. Trace compounds single effect: sulfur compounds**

374 Considering an initial failure of the gas cleaning section ultra-low concentrations of H₂S can reach the cell
 375 during the operation. The possibility to not damage irreversibly the cell was proved from literature results
 376 with a concentration of H₂S below 1 ppm(v) [26,48,49]. The cell was tested at an operating temperature of
 377 750 °C for 50% pre-reformed biogas with a steam-to-carbon ratio equal to 1. An ultra-low concentration of
 378 H₂S (0.46 ppm(v)) was sent to the anode of the cell. The test was carried out over 10 days and the EIS was
 379 performed every 24 h. The ASR starts from 0.71 Ωcm² after 24 h of test and every 24 h the ASR grew by an
 380 average of 2 Ωcm². The final ASR value reached was 0.98 Ωcm².

381

382 An initial voltage drop followed by a steady state cell voltage was observed, as reported also in other
 383 studies [32]. The degradation came about in the first 80 h of operation. In fact, the voltage assumes values
 384 from 0.85 V to 0.74 V in the 240 h of test, but the fastest degradation was recorded in the first 80 h. The long
 385 length of time required to achieve a stable condition is attributed to the low hydrogen sulphide concentration
 386 that determines a longer interval time to cover the first layer of catalytic sites. Sulfur poisoning of the Ni-
 387 anode is a phenomenon that is partially reversible. Once the H₂S flow is stopped, a voltage increase that
 388 suggests S desorption from Ni sites is observed. The desorption trends are quite similar to the corresponding
 389 adsorption trends. As reported by Rasmussen and Hagen (2009), once the H₂S concentration of 2 ppm(v) is
 390 removed the cell performance is completely regenerated [48]. However, above 2 ppm(v) of H₂S, the
 391 performance recovery is not complete. It is likely that some sulfur remains trapped in the three-phase

392 boundary (TPB), thus permanently increasing the anode polarization. This is supported by ASR value and
 393 EIS analysis. It can be seen that the H_2S concentration in time leads to increases in the anode polarization
 394 due to concentration polarization, associated with the transport of gaseous fuel through the anode.



395
 396 *Figure 11. Voltage trend at 10A during 10 days of test with H_2S .*

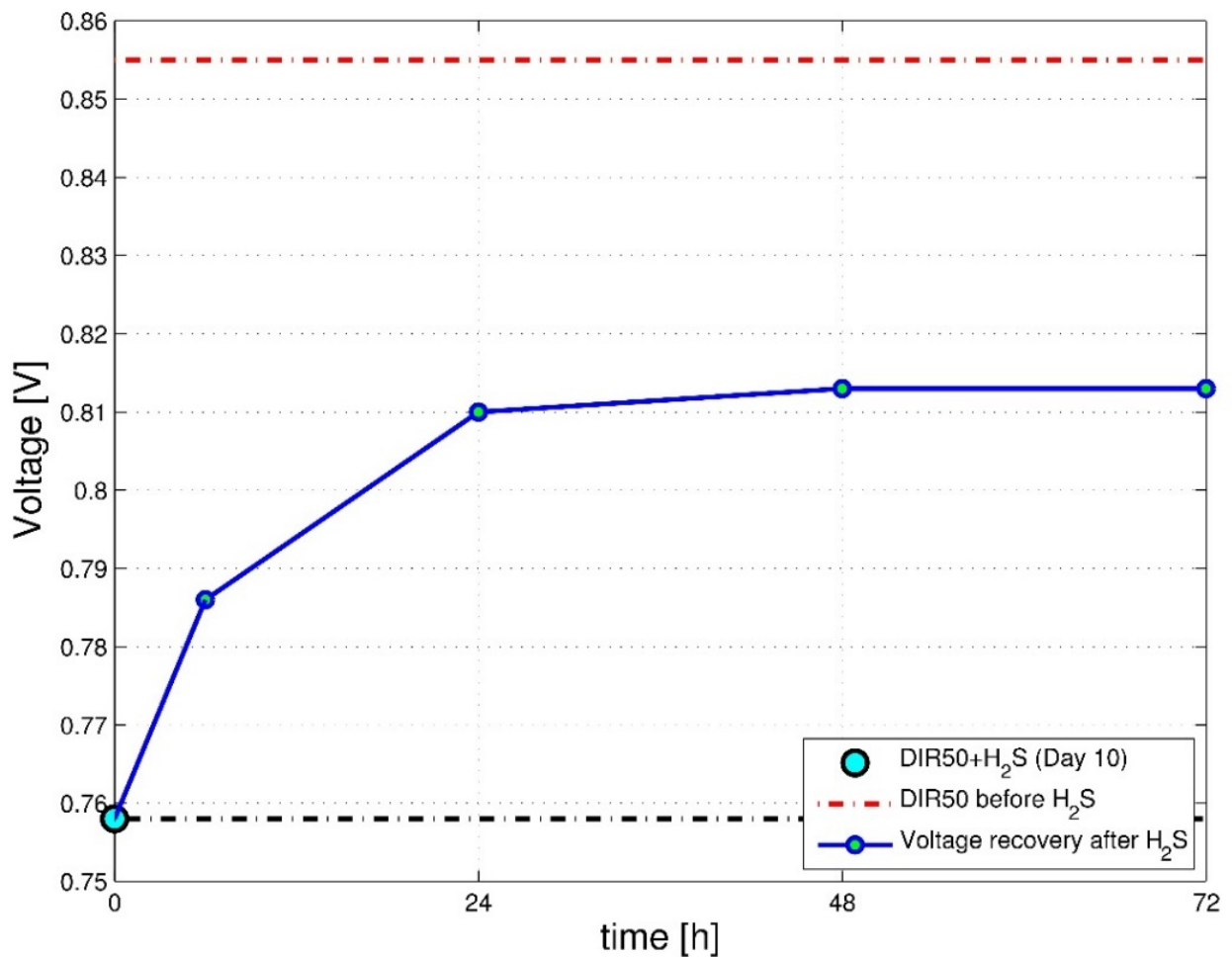
397 The stable condition is reached when the active surface achieves a high percentage of coverage. This
 398 situation determines a lower likelihood for the Sulphur to meet an active site. From this, a slowing in the
 399 coverage phenomenon is recorded. The main cause linked to the increase in the losses can be attributed
 400 overall to an increase in anodic over-potential respect to a variation of the ohmic effect. The main
 401 contribution is related to the low frequency term. This term is mainly affected by the presence of sulfur, this
 402 result is consistent with the results of other studies [50,51]. The frequency range of this arc is consistent with
 403 the range that can be expected for diffusion-related processes [52].

404 The presence of sulphur was found to have a greater effect on reforming reactions than electrochemical
 405 reactions, especially when compared to tests with hydrogen fuel on similar cells and condition [54]. This last
 406 statement allows us to consider the reforming reactions obstructed by the coverage caused by sulphur.
 407 Therefore, it is possible to deduce that the lack in reforming reactions leads to a high amount of no reacting
 408 methane that can take part in the cracking reaction. Consequence of the cracking is that the pores become
 409 blocked. This phenomenon manifests itself through an increase in the second arch of Nyquist plot. In fact,

410 the deposited carbon obstructs the entering of fresh fuel. However, the above mentioned is not the only
 411 reading that can be given at low frequency arch.

412 Recent studies have shown that at SOFC operating temperature, also very small amounts of Sulphur (<1
 413 ppm(v)) can interact with nickel at microstructural level. Prolonged exposure to fuel containing H₂S at
 414 elevated temperatures can lead to Ni coarsening due to adsorption [53]. The growth in Ni particles, results in
 415 loss of percolation and determines the difficulty to spread fresh fuel.

416 The next figure shows that the voltage recovery is around 94% of the value before H₂S administration
 417 (Figure 12). The total voltage recovery is not fully respected because the degradation due to the previous
 418 Sulphur presence was not totally reversible. This occurred both because the adsorbed sulphur is not totally
 419 desorbed from the Ni-sites, as well as because the microstructural changings in Ni were not recovered.



420
 421 *Figure 12. Voltage trend after H₂S removal.*

422 3.2.3. Trace compounds effect: multiple species impact

423 The aim to test the single cell with biogas conditions closer to the reality other pollutants are added to the gas
 424 mixture. These trace compounds are detect in biogas and reported in previous studies, such as siloxanes,
 425 aromatic compounds and terpenes [1].

426

3.2.3.1. Double trace compounds impact on SOFC performance: sulfur and siloxane

427

428

429

430

431

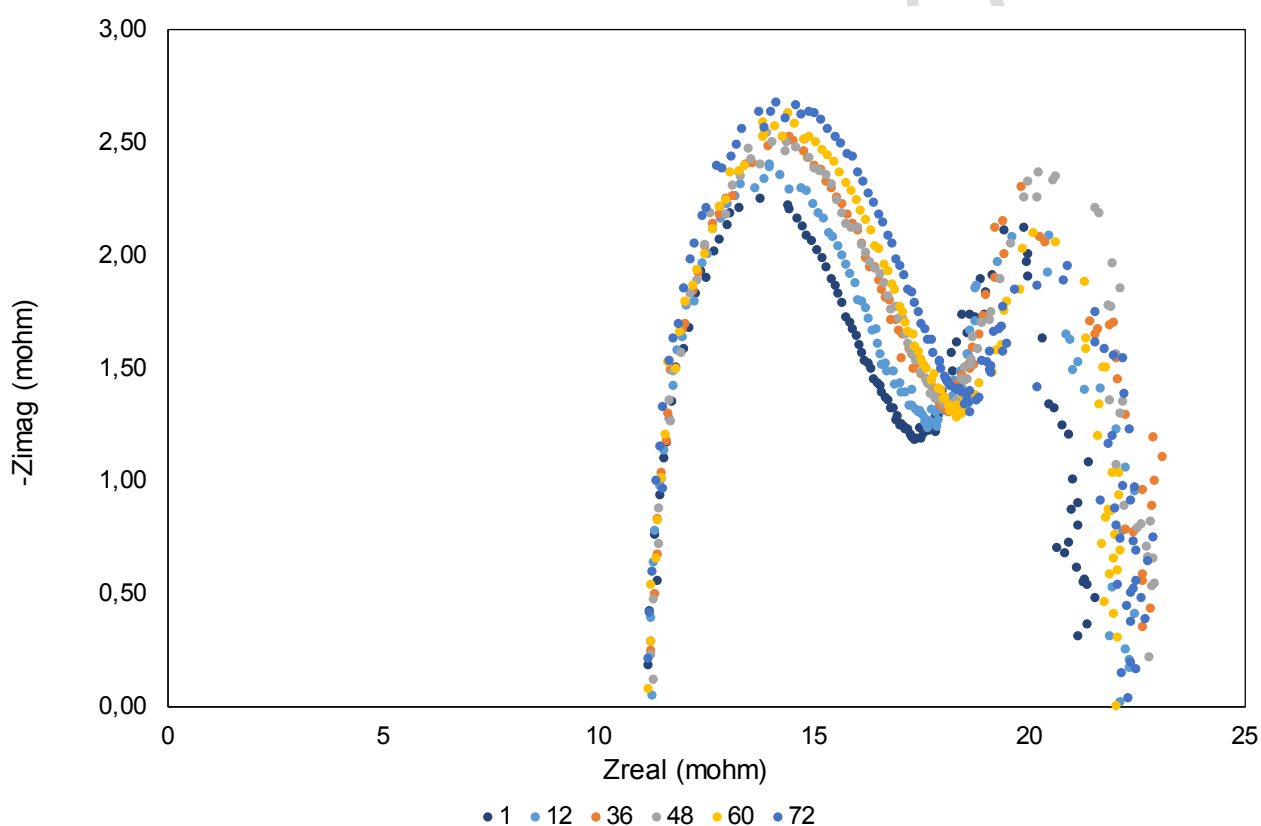
432

433

434

435

Few studies consider the impact of siloxane on SOFC performance but the combined effect with other pollutants are not reported [20,48]. Octamethylcyclotetrasiloxane (D4) was selected as model compound for siloxanes. Siloxanes were detected not only in biogas coming from WWTP, as reported in literature [54,55], but also in biogas coming from organic waste anaerobic digestion process [56]. D4 was detected in biogas coming from the dry anaerobic digestion of OFMSW with a range from 30 to 300 ppb(v). It is known that the more important siloxanes' effect is the formation of SiO_2 . The tested siloxane is contained in certified bottles with 20 ppm(v) of D4 in pure H_2 . The experiments were carried out considering a D4 concentration equal to 0.15 ppm(v) that acts in a period of 72 h. The EIS was carried out with intervals of 12 h and what emerged is shown in the following figure.



436

437

438

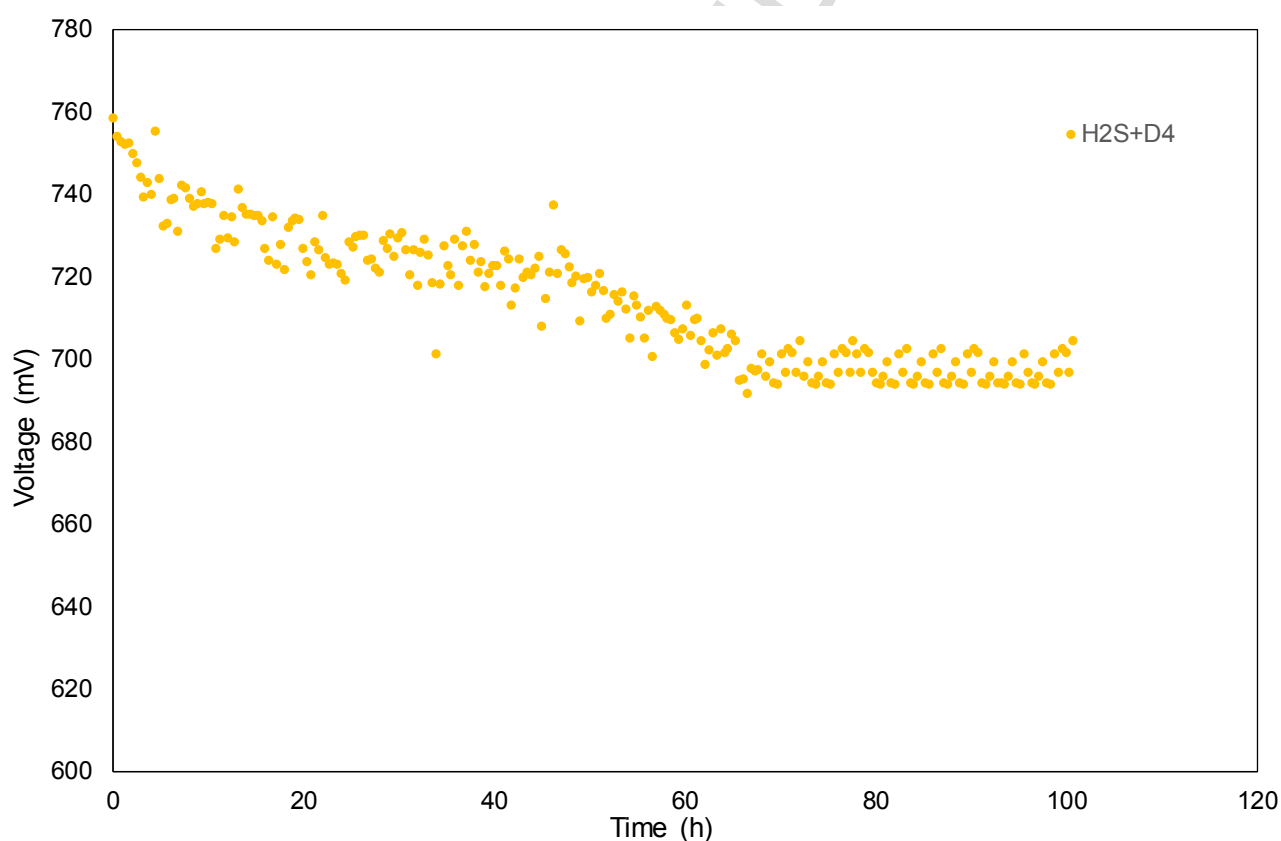
Figure 13. EIS Nyquist diagram for $\text{H}_2\text{S}+\text{D4}$.

Table 8. Losses recorded in the EIS analysis using the electric circuit model approach.

Test condition	Time (h)	R_{ohm} [$\Omega \cdot \text{cm}^2$]	R_{el} [$\Omega \cdot \text{cm}^2$]	R_{tranp} [$\Omega \cdot \text{cm}^2$]	R_p [$\Omega \cdot \text{cm}^2$]
H_2S (last)	240	0.53	0.3	0.15	0.98
$\text{H}_2\text{S}+\text{D4}$	1	0.53	0.3	0.16	0.99

H_2S+D4	72	0.53	0.36	0.21	1.08
-----------	----	------	------	------	------

439 After 1 h of exposure of the second pollutant, the polarization loss assumed a value similar to that
 440 detected in the last test with the H_2S only. The situation appeared to be slightly different after 72 h, when the
 441 increase in the total loss was about $0.09 \Omega \cdot cm^2$ compared to the H_2S case. The losses were due to a 65% to
 442 activation and to a 34% to transportation, determining an increase of $0.06 \Omega \cdot cm^2$ and $0.05 \Omega \cdot cm^2$ in the
 443 high and low frequency arches, respectively. The total losses increased to $0.35 \Omega \cdot cm^2$ compared to the clean
 444 biogas, but $0.25 \Omega \cdot cm^2$ were recorded when only H_2S acts. As other studies confirm [48], Si is able to
 445 deposit and condense not only at the TPB, as happens with Sulphur, but deposits everywhere from the
 446 distribution channel to the interface anode-electrolyte. However, after 72 h a condition of stability had still
 447 not been reached because the D4 acted very slow (the rate is $0.04 V/50 h$). Hence, slow but durable in time
 448 degradation is attributed to silicon that can deposit it everywhere. This mechanism is deleterious from the
 449 SOFC performance point of view; in fact the siloxanes act heavily on the cell decreasing as reported below.



450
 451 *Figure 14. Voltage trend at 10A during 72 h of test with H_2S+D4 .*

452 **3.2.3.2. Triple trace compounds impact on SOFC performance: sulfur, siloxane and**
 453 ***toluene***

454 Another trace compound was added to the gas mixture and cell performance are recorded and reported in
 455 terms of EIS analysis and voltage profile along the test. The considered TAR was the toluene (C_7H_8). This is

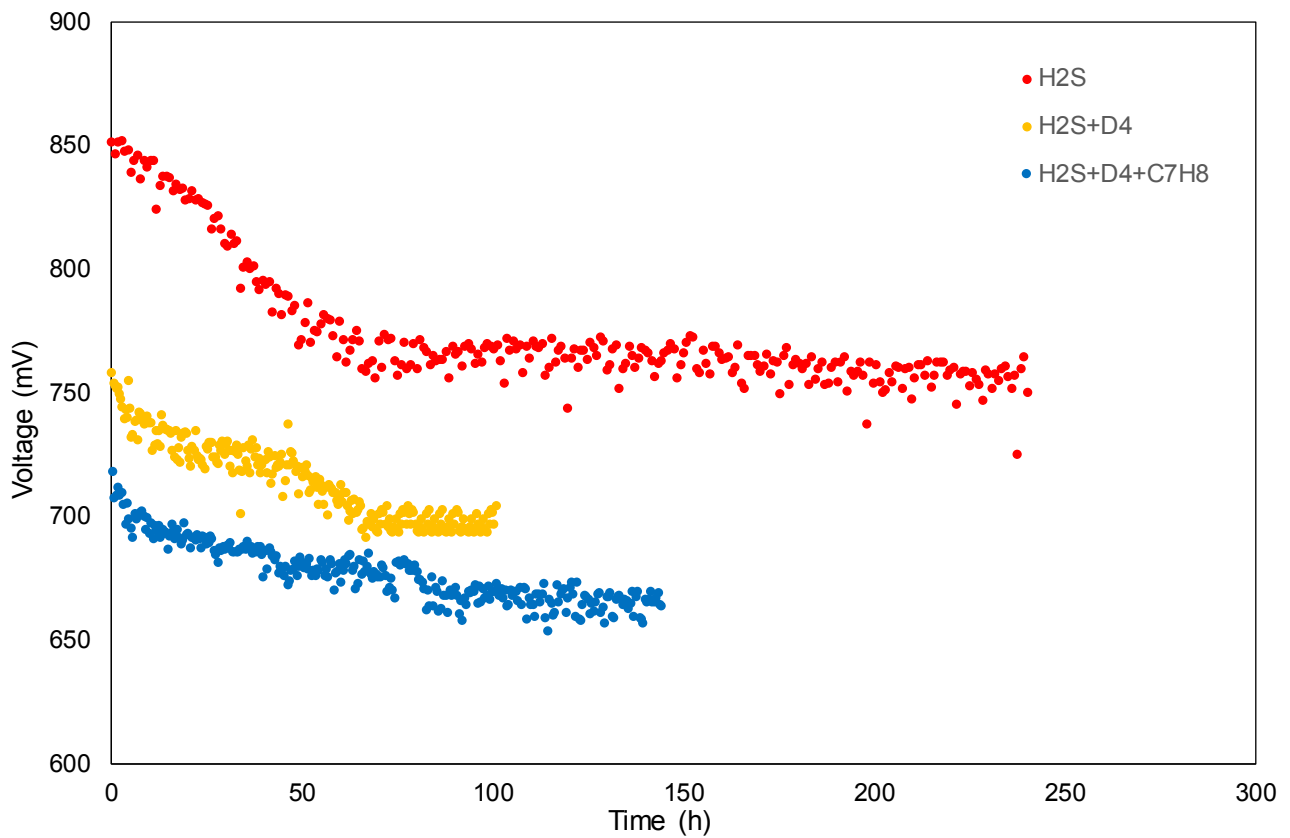
456 one of the lightest TAR compounds and it can be easily detected in biogas from organic waste [1,5]. Toluene
457 is one of the TAR with the lower molecular weight thus highly reactive, for this reason, it represents the
458 worst condition for the cell operation.

459 The SOFC was fed with a concentration of toluene equal to 45.7 ppm(v). The tests were carried out over
460 six days, and the EIS was performed at intervals of 24 h each. As for the ohmic contribution, no variations
461 were recorded. However, the overall polarization tended to increase.

462 Losses increase of $0.15 \Omega \cdot \text{cm}^2$ and mostly affect the low frequency arch of Nyquist plot. This last
463 aspect is verifiable observing that the high frequencies account only for 20% of the total. Considering all the
464 pollutants introduced, the C_7H_8 had the highest consequences on the diffusivity of fresh fuel at the anode.

465 Being the second arch related to the mass transport mechanisms, carbon deposition could have occurred.
466 This hypothesis is also confirmed by previous studies [20]. The presence of hydrocarbons in the biogas feed
467 could lead to the the cracking of molecules. This situation induces a decrease in the active sites that are
468 normally the promoter of reforming or electrochemical reactions. Under these conditions, methane is more
469 prone to take part in the cracking reaction compared to the reforming reactions. The carbon released by
470 cracking is deposited in the anode layer, so obstructing the inlet of fresh fuel.

471 The low-frequency arch, as already specified, is also affected by the H_2S impact, even if this produces
472 consequences that are not alarming. In fact, the losses related to combined effect accounts for $0.15 \Omega \cdot \text{cm}^2$ in
473 the most degraded condition, otherwise, the only H_2S effect is of $0.02 \Omega \cdot \text{cm}^2$. This means that, the losses
474 related to the C_7H_8 assume values around $0.12 \Omega \cdot \text{cm}^2$. Considering Figure 15 the voltage profile shows the
475 cell performance decreasing when three different trace compounds are added to the SOFC cell. The
476 performance achieved are quite stable at the end, this demonstrates how the cell is not broken but it is
477 irreversibly affected by the trace compounds considered, when these compounds are removed from the gas
478 mixture, see Figure 16.



479

480

Figure 15. Voltage trend at 10A during 6 days of test with $H_2S+D_4+C_7H_8$.

481

482

Figure 16 shows the iV curve made at the beginning of the test and after the removal of trace compounds, demonstrating that the SOFC performance are irreversibly affected.

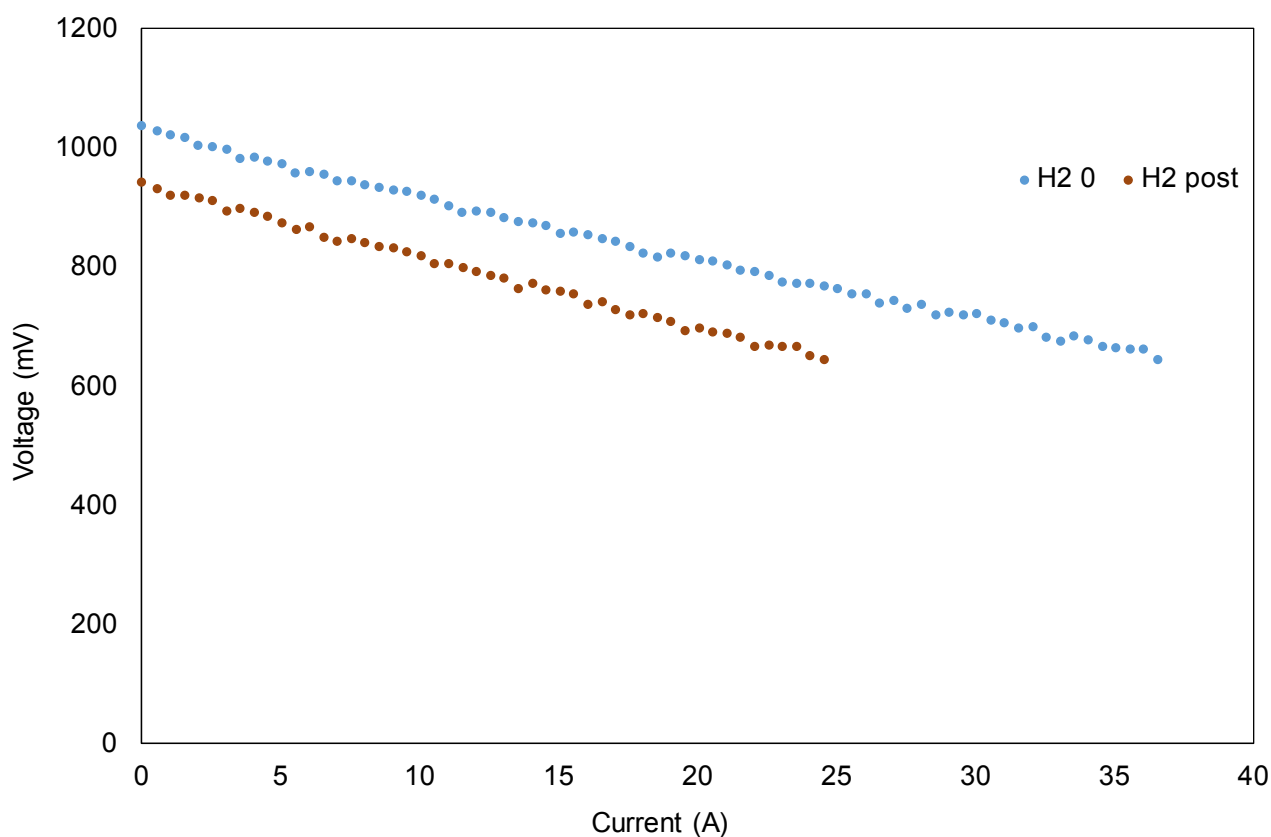


Figure 16. *iV* curve in hydrogen made at the beginning and at the end of the test session.

4. Conclusions

A Ni/Al₂O₃ catalyst appears suitable for the steam reforming of biogas including contaminants, under the operative conditions adopted (CH₄/CO₂=60/40 vol.%, T=1073 K, H₂O/CH₄=2 mol/mol and GHSV=15,000 h⁻¹). Some tolerance towards the presence of one or more poisoning compounds in the inlet gas stream has been shown (among H₂S≤0.4 ppm(v), C₂-C₃ hydrocarbons mixture ≤200 ppm(v), and D5≤0.5 ppm(v)). The combined effect of two poisoning compounds in the feed does not seem to affect the Ni catalyst stability (if the concentration of the contaminants are below a threshold limit) when the biogas is composed of a methane to carbon dioxide ratio >1 under the tested operating conditions.

On the contrary, the effect of a biogas stream with composition CH₄/CO₂=50/50 vol. % is much more harmful under steam reforming conditions both in terms of activity and stability, probably due mainly to the CO₂-promoted Boudouard reaction that leads to extensive carbon formation on the catalyst surface. Under this condition, sulfur and D5 compounds in the biogas have a significant impact on the longevity of the Ni catalyst. Hence, the carbon formation rate is affected by the degree of catalyst poisoning due to adsorption and/or deposition of other species (i.e. sulfur and/or silicon oxide) on catalytic sites.

The Ni-anode SOFC performance was investigated varying the DIR condition and testing the impact of trace compounds. DIR investigation proved that the single cell was able to withstand stable up to DIR 50. The best

502 performance was achieved in this condition given the low H_2O/H_2 ratio that allows to obtain a high-
503 performance operation because reactants do not lower their partial pressure at the anode. At the same time a
504 suitable H_2O/CH_4 ratio should be present because the reforming reactions take place. The combinations
505 from these conditions are well verified in the DIR50 condition.

506 Considering the trace compounds impact on SOFC performance, H_2S single compound plus D4 and C_7H_8 as
507 model compounds for sulfurs, siloxanes, and aromatic compounds were investigated. Some conclusions are
508 resumed below, considering the EIS analysis:

- 509 • Ohmic losses: the presence of any species of contaminant in the feeding biogas does not damage the
510 electrolytic layer that preserves unchanged its conductive characteristics.
- 511 • Activation Losses: the drop in the activation losses is recorded to reach the highest value when the
512 H_2S is sent to the anode, in fact, the increasing of the activation losses is of $0.26 \Omega \cdot cm^2$. Even if C_7H_8 and
513 D4 have an influence on the performance, they produce an increase in losses equal to $0.03 \Omega \cdot cm^2$ and 0.04
514 $\Omega \cdot cm^2$, respectively. The justification linked to these behaviours can be found on the effect that each
515 pollutant produces, i.e. the adsorption/desorption in the catalytic sites and the capability to deposit itself
516 everywhere in the cell structure, respectively.
- 517 • Transportation losses: the low frequency arch of the Nyquist plot is mostly affected by the presence
518 of C_7H_8 , while the D4 concentration, below 150 ppb(v) and H_2S do not influence most this loss. In fact, the
519 aromatic compound leads to an increase in the losses of about $0.12 \Omega \cdot cm^2$ compared to the case when only
520 D4 and H_2S act. This is mostly due to the carbon deposition that follows the reduced capacity of Ni sites to
521 promote reforming reactions.

522

523 Acknowledgements

524 This research is a part of the DEMOSOFC project (European project FCH2 JU – grant number
525 671470).

526

527 References

- 528 [1] Papurello D, Soukoulis C, Schuhfried E, Cappellin L, Gasperi F, Silvestri S, et al. Monitoring of
529 volatile compound emissions during dry anaerobic digestion of the Organic Fraction of Municipal
530 Solid Waste by Proton Transfer Reaction Time-of-Flight Mass Spectrometry. *Bioresour. Technol.*,
531 vol. 126, 2012, p. 254–65.
- 532 [2] Papurello D, Silvestri S, Tomasi L, Belcari I, Biasioli F. Natural gas trace compounds analysis with
533 innovative systems: PTR-ToF-MS and FASTGC. *Energy Procedia* 2016;101:536–41.
534 doi:10.1016/j.egypro.2016.11.068.

- 535 [3] Papurello D, Schuhfried E, Lanzini A, Romano A, Cappellin L, Märk TD, et al. Proton transfer
536 reaction-mass spectrometry as a rapid inline tool for filter efficiency of activated charcoal in support
537 of the development of Solid Oxide Fuel Cells fueled with biogas. *Fuel Process Technol* 2015;130:78–
538 86. doi:10.1016/j.fuproc.2014.09.042.
- 539 [4] Papurello D, Lanzini A, Leone P, Santarelli M, Silvestri S. Biogas from the organic fraction of
540 municipal solid waste: Dealing with contaminants for a solid oxide fuel cell energy generator. *Waste*
541 *Manag* 2014;34:2047–56.
- 542 [5] Rasi S, Veijanen a., Rintala J. Trace compounds of biogas from different biogas production plants.
543 *Energy* 2007;32:1375–80. doi:10.1016/j.energy.2006.10.018.
- 544 [6] Statheropoulos M, Agapiou A, Pallis G. A study of volatile organic compounds evolved in urban
545 waste disposal bins. *Atmos Environ* 2005;39:4639–45. doi:10.1016/j.atmosenv.2005.04.013.
- 546 [7] Allen MR, Braithwaite A, Hills CC. Trace Organic Compounds in Landfill Gas at Seven U . K .
547 Waste Disposal Sites 1997;31:1054–61.
- 548 [8] Papurello D, Silvestri S, Tomasi L, Belcari I, Biasioli F, Santarelli M. Biowaste for SOFCs. *Energy*
549 *Procedia* 2016;101:424–31. doi:10.1016/j.egypro.2016.11.054.
- 550 [9] Rasi S, Lântelä J, Rintala J. Trace compounds affecting biogas energy utilisation - A review. *Energy*
551 *Convers Manag* 2011;52:3369–75. doi:10.1016/j.enconman.2011.07.005.
- 552 [10] Papurello D, Lanzini A, Schufried E, Santarelli M, Silvestri S. Proton Transfer Reaction-Mass
553 Spectrometry (PTR-MS) as a rapid online tool for biogas VOCs monitoring in support of the
554 development of Solid Oxide Fuel Cells (SOFCs). 6th Int PTR-MS Conf 2013;130:144–50.
555 doi:10.1016/j.fuproc.2014.09.042.
- 556 [11] Papurello D, Schuhfried E, Lanzini A, Romano A, Cappellin L, Märk TD, et al. Influence of co-
557 vapors on biogas filtration for fuel cells monitored with PTR-MS (Proton Transfer Reaction-Mass
558 Spectrometry). *Fuel Process Technol* 2014;118:133–40. doi:10.1016/j.fuproc.2013.08.011.
- 559 [12] Papurello D, Tomasi L, Silvestri S, Santarelli M. Evaluation of the Wheeler-Jonas parameters for
560 biogas trace compounds removal with activated carbons. *Fuel Process Technol* 2016;152:93–101.
561 doi:10.1016/j.fuproc.2016.06.006.
- 562 [13] Papurello D, Tognana L, Lanzini A, Smeacetto F, Santarelli M, Belcari I, et al. Proton transfer
563 reaction mass spectrometry technique for the monitoring of volatile sulfur compounds in a fuel cell
564 quality clean-up system. *Fuel Process Technol* 2015;130:136–46. doi:10.1016/j.fuproc.2014.09.041.
- 565 [14] Papurello D, Tomasi L, Silvestri S, Belcari I, Santarelli M, Smeacetto F, et al. Biogas trace compound
566 removal with ashes using proton transfer reaction time-of-flight mass spectrometry as innovative
567 detection tool. *Fuel Process Technol* 2016;145:62–75. doi:10.1016/j.fuproc.2016.01.028.
- 568 [15] Papurello D, Boschetti A, Silvestri S, Khomenko I. Real-time monitoring of removal of trace
569 compounds with PTR-MS: Biochar experimental investigation. *Renew Energy* 2018.
570 doi:10.1016/j.renene.2018.02.122.
- 571 [16] Nam S, Namkoong W, Kang J, Park J, Lee N. Adsorption characteristics of siloxanes in landfill gas
572 by the adsorption equilibrium test. *Waste Manag* 2013;33:2091–8.
573 doi:10.1016/j.wasman.2013.03.024.
- 574 [17] Lodewyckx P, Verhoeven L. Using the modified Wheeler-Jonas equation to describe the adsorption
575 of inorganic molecules: Chlorine. *Carbon N Y* 2003;41:1215–9. doi:10.1016/S0008-6223(03)00052-
576 6.
- 577 [18] Van Herle J, Membrez Y, Bucheli O. Biogas as a fuel source for SOFC co-generators. *J Power*

- 578 Sources 2004;127:300–12. doi:10.1016/j.jpowsour.2003.09.027.
- 579 [19] Papurello D, Lanzini A, Tognana L, Silvestri S, Santarelli M. Waste to energy: Exploitation of biogas
580 from organic waste in a 500 W solid oxide fuel cell (SOFC) stack. *Energy* 2015;85:145–58.
581 doi:10.1016/j.energy.2015.03.093.
- 582 [20] Papurello D, Lanzini A, Drago D, Leone P, Santarelli M. Limiting factors for planar solid oxide fuel
583 cells under different trace compound concentrations. *Energy* 2016;95:67–78.
584 doi:10.1016/j.energy.2015.11.070.
- 585 [21] Chavez R-H, Guadarrama JJ, Kastner JR, Das KC, Buquoi Q, Melear ND. Biogas treatment by ashes
586 from incineration processes. *Clean Technol Environ Policy* 2003;37:2568–74. doi:10.1007/s10098-
587 015-0980-3.
- 588 [22] Galvagno A, Chiodo V, Urbani F, Freni F. Biogas as hydrogen source for fuel cell applications. *Int J*
589 *Hydrogen Energy* 2013;38:3913–20. doi:10.1016/j.ijhydene.2013.01.083.
- 590 [23] Chiodo V, Galvagno A, Lanzini A, Papurello D, Urbani F, Santarelli M, et al. Biogas reforming
591 process investigation for SOFC application. *Energy Convers Manag* 2015;98:252–8.
592 doi:10.1016/j.enconman.2015.03.113.
- 593 [24] Effendi A, Zhang ZG, Hellgardt K, Honda K, Yoshida T. Steam reforming of a clean model biogas
594 over Ni/Al₂O₃ in fluidized- and fixed-bed reactors. *Catal. Today*, vol. 77, 2002, p. 181–9.
595 doi:10.1016/S0920-5861(02)00244-4.
- 596 [25] Rostrup-Nielsen J, Bak Hansen J-H. CO₂-Reforming of Methane over Transition Metals. *J Catal*
597 1993;144:38–49. doi:10.1006/jcat.1993.1312.
- 598 [26] Izquierdo U, Barrio VL, Lago N, Requies J, Cambra JF, Gemez MB, et al. Biogas steam and
599 oxidative reforming processes for synthesis gas and hydrogen production in conventional and
600 microreactor reaction systems. *Int. J. Hydrogen Energy*, vol. 37, 2012, p. 13829–42.
601 doi:10.1016/j.ijhydene.2012.04.077.
- 602 [27] Avraam DG, Halkides TI, Liguras DK, Bereketidou OA, Goula MA. An experimental and theoretical
603 approach for the biogas steam reforming reaction. *Int. J. Hydrogen Energy*, vol. 35, 2010, p. 9818–27.
604 doi:10.1016/j.ijhydene.2010.05.106.
- 605 [28] Appari S, Janardhanan VM, Bauri R, Jayanti S. Deactivation and regeneration of Ni catalyst during
606 steam reforming of model biogas: An experimental investigation. *Int J Hydrogen Energy*
607 2014;39:297–304. doi:10.1016/j.ijhydene.2013.10.056.
- 608 [29] Galvagno A, Chiodo V, Urbani F, Freni F. Biogas as hydrogen source for fuel cell applications. *Int J*
609 *Hydrogen Energy* 2013;38:3913–20. doi:10.1016/j.ijhydene.2013.01.083.
- 610 [30] Chiodo V, Urbani F, Galvagno A, Mondello N, Freni S. Analysis of biogas reforming process for
611 molten carbonate fuel cells. *J Power Sources* 2012;206:215–21. doi:10.1016/j.jpowsour.2012.01.114.
- 612 [31] Ashrafi M, Pfeifer C, Pröll T, Hofbauer H. Experimental study of model biogas catalytic steam
613 reforming: 2. Impact of sulfur on the deactivation and regeneration of Ni-based catalysts. *Energy and*
614 *Fuels* 2008;22:4190–5. doi:10.1021/ef8000828.
- 615 [32] Papurello D, Lanzini A, Fiorilli S, Smeacetto F, Singh R, Santarelli M. Sulfur poisoning in Ni-anode
616 solid oxide fuel cells (SOFCs): Deactivation in single cells and a stack. *Chem Eng J* 2016;283:1224–
617 33. doi:10.1016/j.cej.2015.08.091.
- 618 [33] Papurello D, Borchiellini R, Bareschino P, Chiodo V, Freni S, Lanzini A, et al. Performance of a
619 Solid Oxide Fuel Cell short-stack with biogas feeding. *Appl Energy* 2014;125:254–63.

- 620 [34] Ereksn EJ, Bartholomew CH. Sulfur poisoning of nickel methanation catalysts. II. Effects of H₂S
621 concentration, CO and H₂O partial pressures and temperature on reactivation rates. *Appl Catal*
622 1983;5:323–36. doi:10.1016/0166-9834(83)80160-2.
- 623 [35] Papurello D, Lanzini A, Drago D, Leone P, Santarelli M. Limiting factors for planar solid oxide fuel
624 cells under different trace compound concentrations. *Energy* 2016;95:67–78.
625 doi:10.1016/j.energy.2015.11.070.
- 626 [36] Abild-Pedersen F, Lytken O, Engbæk J, Nielsen G, Chorkendorff I, Nørskov JK. Methane activation
627 on Ni(1 1 1): Effects of poisons and step defects. *Surf Sci* 2005;590:127–37.
628 doi:10.1016/j.susc.2005.05.057.
- 629 [37] Sidjabat O, Trimm DL. Nickel-magnesia catalysts for the steam reforming of light hydrocarbons. *Top*
630 *Catal* 2000;11–12:279–82. doi:10.1023/A:1027212301077.
- 631 [38] Hofmann P, Panopoulos KD, Fryda LE, Schweiger A, Ouweltjes JP, Karl J. Integrating biomass
632 gasification with solid oxide fuel cells: Effect of real product gas tars, fluctuations and particulates on
633 Ni-GDC anode. *Int J Hydrogen Energy* 2008;33:2834–44. doi:10.1016/j.ijhydene.2008.03.020.
- 634 [39] Hofmann P, Panopoulos KD, Aravind P V., Siedlecki M, Schweiger A, Karl J, et al. Operation of
635 solid oxide fuel cell on biomass product gas with tar levels. *Int J Hydrogen Energy* 2009;34:9203–12.
636 doi:10.1016/j.ijhydene.2009.07.040.
- 637 [40] Trimm DL. Catalyst design for reduced coking (review). *Appl Catal* 1983;5:263–90.
638 doi:10.1016/0166-9834(83)80156-0.
- 639 [41] Sidjabat O, Trimm DL. Nickel-magnesia catalysts for the steam reforming of light hydrocarbons. *Top*
640 *Catal* 2000;11–12:279–82. doi:10.1023/A:1027212301077.
- 641 [42] Angeli SD, Pilitsis FG, Lemonidou AA. Methane steam reforming at low temperature: Effect of light
642 alkanes' presence on coke formation. *Catal Today* 2015;119–28. doi:10.1016/j.cattod.2014.05.043.
- 643 [43] Chiodo V, Urbani F, Galvagno A, Mondello N, Freni S. Analysis of biogas reforming process for
644 molten carbonate fuel cells. *J Power Sources* 2012;206:215–21. doi:10.1016/j.jpowsour.2012.01.114.
- 645 [44] Papurello D, Lanzini A, Leone P, Santarelli M. The effect of heavy tars (toluene and naphthalene) on
646 the electrochemical performance of an anode-supported SOFC running on bio-syngas. *Renew Energy*
647 2016;99:747–53. doi:10.1016/j.renene.2016.07.029.
- 648 [45] Abild-Pedersen F, Lytken O, Engbæk J, Nielsen G, Chorkendorff I, Nørskov JK. Methane activation
649 on Ni(1 1 1): Effects of poisons and step defects. *Surf Sci* 2005;590:127–37.
650 doi:10.1016/j.susc.2005.05.057.
- 651 [46] Didenko LP, Savchenko VI, Arutyunov VS, Sementsova LA. Steam reforming of methane mixtures
652 with ethylene over an industrial nickel catalyst. *Pet Chem* 2008;48:22–7. doi:10.1007/s11494-008-
653 1004-x.
- 654 [47] Haga K, Adachi S, Shiratori Y, Itoh K, Sasaki K. Poisoning of SOFC anodes by various fuel
655 impurities. *Solid State Ionics* 2008;179:1427–31. doi:10.1016/j.ssi.2008.02.062.
- 656 [48] Madi H, Lanzini A, Diethelm S, Papurello D, Van herle J, Lualdi M, et al. Solid oxide fuel cell anode
657 degradation by the effect of siloxanes. *J Power Sources* 2015;279:460–71.
658 doi:10.1016/j.jpowsour.2015.01.053.
- 659 [49] Choudhary V., Uphade B., Mamman A. Simultaneous steam and CO₂ reforming of methane to
660 syngas over NiO/MgO/SA-5205 in presence and absence of oxygen. *Appl Catal A Gen* 1998;168:33–
661 46. doi:10.1016/S0926-860X(97)00331-1.

- 662 [50] Avraam DG, Halkides TI, Liguras DK, Bereketidou OA, Goula MA. An experimental and theoretical
663 approach for the biogas steam reforming reaction. *Int. J. Hydrogen Energy*, vol. 35, 2010, p. 9818–27.
664 doi:10.1016/j.ijhydene.2010.05.106.
- 665 [51] Delahay G, Duprez D. Effect of sulphur on the coking of rhodium in the steam reforming of 1-
666 methyl-naphthalene. *Appl Catal* 1989;53:95–105. doi:10.1016/S0166-9834(00)80014-7.
- 667 [52] Strohm JJ, Zheng J, Song C. Low-temperature steam reforming of jet fuel in the absence and
668 presence of sulfur over Rh and Rh-Ni catalysts for fuel cells. *J Catal* 2006;238:309–20.
669 doi:10.1016/j.jcat.2005.12.010.
- 670 [53] Leone P, Matencio T, Garcia ME, Domigues ZR, Lanzini A, Santarelli M. Limiting Factors for a
671 Planar Solid Oxide Fuel Cell Under Different Flow and Temperature Conditions. *Fuel Cells* 2013:n/a-
672 n/a. doi:10.1002/fuce.201200154.
- 673 [54] Rasmussen JFB, Hagen A. The effect of H₂S on the performance of Ni-YSZ anodes in solid oxide
674 fuel cells. *J Power Sources* 2009;191:534–41. doi:10.1016/j.jpowsour.2009.02.001.
- 675 [55] Rasmussen JFB, Hagen A. The Effect of H₂S on the Performance of SOFCs using Methane
676 Containing Fuel 2010:1135–42. doi:10.1002/fuce.201000012.
- 677 [56] Zha S, Cheng Z, Liu M. Sulfur Poisoning and Regeneration of Ni-Based Anodes in Solid Oxide Fuel
678 Cells. *J Electrochem Soc* 2007;154:B201–6. doi:10.1149/1.2404779.
- 679 [57] Cheng Z, Zha S, Liu M. Influence of cell voltage and current on sulfur poisoning behavior of solid
680 oxide fuel cells. *J Power Sources* 2007;172:688–93. doi:10.1016/j.jpowsour.2007.07.052.
- 681 [58] Aravind PV, Ouweltjes JP, Schoonman J. Diffusion Impedance on Nickel/Gadolinia-Doped Ceria
682 Anodes for Solid Oxide Fuel Cells. *J Electrochem Soc* 2009;156:B1417–22. doi:10.1149/1.3231490.
- 683 [59] Ivey DG, Brightman E, Brandon N. Structural modifications to nickel cermet anodes in fuel cell
684 environments. *J Power Sources* 2010;195:6301–11. doi:10.1016/j.jpowsour.2010.04.059.
- 685 [60] Arnold M, Kajolinna T. Development of on-line measurement techniques for siloxanes and other
686 trace compounds in biogas. *Waste Manag* 2010;30:1011–7. doi:10.1016/j.wasman.2009.11.030.
- 687 [61] Arnold M. Reduction and monitoring of biogas trace compounds. 2009.

688

Highlights

- Ni catalyst stability is achieved with biogas mixture with $\text{CH}_4/\text{CO}_2 > 1$
- $\text{CH}_4/\text{CO}_2 = 50/50$ vol. % is much more harmful under steam reforming conditions both in terms of activity and stability
- The impact of trace contaminants not removed from the cleaning section from biogas are investigated on SOFCs